Anomalous deviations from statistical evaporation spectra for the decay of the ^{73}Br and ^{77}Rb compound systems

Maninder Kaur, B. R. Behera,[*] Gulzar Singh, Varinderjit Singh,[†] Rohit Sandal,[‡] A. Kumar, H. Singh,[§] Gurpreet Singh, and K. P. Singh
Department of Physics, Panjab University, Chandigarh 160014, India

N. Madhavan, S. Nath, A. Jhingan, J. Gehlot, K. S. Golda, and P. Sugathan
Inter University Accelerator Centre, Aruna Asaf Ali Marg, New Delhi 110067, India

Davinder Siwal and Sunil Kalkal[†]
Department of Physics and Astrophysics, University of Delhi, Delhi 110007, India

E. Prasad[‖]
Department of Physics, University of Calicut 673635, India

S. Appannababu[¶]
Department of Physics, Faculty of Science, The M. S. University of Baroda, Vadodara 390002, India
(Received 9 August 2013; revised manuscript received 12 February 2014; published 26 March 2014)

Background: Several inclusive and few exclusive [evaporation residue (ER) gated] measurements for symmetric systems reported in the literature describe the anomalous deviations of light particle evaporation spectra from the statistical model predictions. However, no consistent description exists for these deviations.
Purpose: To establish the consistent interpretation of reported anomalous deviations.
Method: The inclusive and exclusive measurements of α-particle, proton, and neutron spectra were carried out for the fusion of two relatively symmetric systems ^{28}Si + ^{45}Sc ($E_{\rm lab} = 125$ MeV and $l_{\rm max} = 47\hbar$) and ^{32}S + ^{45}Sc ($E_{\rm lab} = 125$ MeV and $l_{\rm max} = 43\hbar$) leading to the compound nuclei ^{73}Br and ^{77}Rb with excitation energies 78 MeV and 71 MeV, respectively.
Results: The experimental light particle spectra for both the reactions show anomalous deviations from the statistical model predictions. The charged particles spectra are found to be suppressed, whereas the neutron spectra exhibit a bump at the higher energy tail. These spectra are investigated in terms of the modification of the important ingredients of the statistical model viz. the level density parameter, rescaling of the yrast line, and the use of l value suggested by the dynamical models.
Conclusions: It is conjectured that the higher partial waves do not fuse, but result in the formation of a deformed dinuclear system. The binding energy of neutrons is reduced while those for protons and α particles are enhanced in the deformed dinuclear system as compared to those in the shape-equilibrated system. Hence, the higher partial waves inhibit their contributions to the α-particle spectra and lead to the preshape equilibrium of neutrons and protons, with the neutron emission dominating over the proton emission.

DOI: 10.1103/PhysRevC.89.034621 PACS number(s): 25.70.Jj, 25.70.Gh, 24.10.Pa

I. INTRODUCTION

Heavy ion induced fusion reactions populate compound nuclei (CN) with high excitation energies and angular momenta. For projectile energy above 10 MeV/nucleon, fusing nuclei reseparate before the formation of a fully equilibrated CN. However, at low energy the formation of CN becomes a dominant process. The hot rotating CN undergoes sequential decay through fission or emission of α particles, protons, and neutrons. The high angular momentum states decay preferentially through α-particle emission (or fission in the case of heavy CN) while the lower angular momentum states decay through proton or neutron emission. These light particles carry important signatures about the underlying reaction mechanism of the fusion process. The statistical model has been extensively used to explain the light particle evaporation spectra and to extract information about the nuclear level density and barrier penetration probability. Several experimental studies [1–10] suggest that the light charged particles and neutron spectra from mass symmetric projectile-target systems show significant deviations from those predicted by

[*]Corresponding author: bivash@pu.ac.in
[†]Present address: Centre for Physical and Mathematical Sciences, Central University of Punjab, Bathinda 151001, India.
[‡]Present address: Department of Physics, S.V. Government College Ghumarwin, Bilaspur (H.P.) 174021, India.
[§]Present address: Department of Physics, Kurukshetra University, Kurukshetra, Haryana 136119, India.
[‖]Present address: Department of Physics, School of Mathematical and Physical Sciences, Central University of Kerala, Kasaragod 671314, India.
[¶]Present address: INFN, Laboratori Nazionali di Legnaro, I-35020 Legnaro (Padova), Italy.

the statistical model calculations using the rotating liquid drop model (RLDM) moment of inertia, the transmission coefficients from the optical model for spherical nuclei, level density parameter 'a' $= A/8$ MeV^{-1} and the maximum value of angular momentum, $l = l_{\max}$.[1] The deviations at the lower energy side of the peak of evaporation spectra are explained by lowering the emission barrier as compared to the inverse absorption channels owing to large deformations at higher excitation energy and angular momentum [11,12]. Anomalous deviations from the statistical model are also observed at the higher energy tail of the evaporation spectra. The higher energy tail of the charged particles spectra are softer while for the neutrons the spectra are harder in comparison to the statistical model predictions and exhibit a bump which is a critical signature for pre-equilibrium process [13]. The deviation of α-particle spectra has been explained using different methods like the modification of spin dependent level density or optimizing the deformation parameters [14–17]. However, these methods failed to explain the proton spectra for some target-projectile combinations [2,3,16]. It was suggested that the proton deviations may be due to the contributions from pre-equilibrium processes. In another approach to explain anomalous deviations, the dynamical model based code HICOL [18] was used. It suggests that the fusion of higher partial waves for the mass symmetric entrance channels is strongly hindered. The l value suggested by this model, which is less than the classical $l = l_{\max}$, explains the deviations for the α-particle spectra [2–7], however still the proton spectra could not be explained in certain cases [2,3].

For the neutron spectra, anomalous behavior could not be explained either by using the HICOL predicted l values or the modification of the spin dependent level density. In some studies, attempts have been made to reproduce the spectra by using the lower value of 'a' and the observed behavior was explained in terms of pre-equilibrium emission owing to high temperature of the nonequilibrated system [8–10]. But at the same time, it is found that the thermal equilibrium is very fast whereas the shape equilibrium is delayed [3–6,19], so there should not be any localized high temperature region in the composite system. Hence the interpretation given by the authors for the pre-equilibrium emission does not seem to be satisfactory.

In the whole scenario, it can be concluded that no consistent picture exists which explains the anomalous deviations for all the light particle evaporation spectra simultaneously. Moreover most of the earlier measurements performed in this direction are inclusive measurements and exclusive measurements with the ER gating are scarce. Therefore it is essential to carry out refined exclusive simultaneous measurements to minimize the possibility of nonstatistical processes and to do a critical shape analysis of the light particle evaporation spectra. To explore these aspects in a better way, we have preformed the exclusive (ER gated) measurements of α-particle, proton, and neutron evaporation spectra for the decay of ^{73}Br and ^{77}Rb CN produced in the heavy ion induced fusion reactions of two relatively symmetric systems ^{28}Si + ^{45}Sc and ^{32}S + ^{45}Sc. As the heavy ion induced fusion reaction is one of the most drastic rearrangements that a many-body system may undergo, so the detailed applications of dynamical models [18,20,21] in addition to the statistical model enabled us to understand the details of the reaction mechanism and develop a consistent picture of the deviations from the statistical model. The present work reports the analysis of experimental results in terms of both the statistical and dynamical model calculations.

The present article is organized in the following way. The experimental setup and data analysis is described in Sec. II followed by the details of the theoretical analysis and results in Sec. III. Section IV contains the discussion and finally the summary and conclusions are presented in Sec. V.

II. EXPERIMENTAL SETUP AND DATA ANALYSIS

The experiment was performed using Heavy Ion Reaction Analyzer (HIRA) [22] facility at Inter University Accelerator Centre (IUAC), New Delhi. The pulsed beams of ^{28}Si and ^{32}S (pulse separation of 1 μs) and $E_{\rm lab} = 125$ MeV were obtained from the 15UD pelletron accelerator. The self-supporting target of ^{45}Sc (of thickness 520 μg/cm^2) was prepared by the rolling technique. The CN ^{73}Br was populated with an excitation energy of 78 MeV and $l_{\max} = 47\hbar$ through the ^{28}Si + ^{45}Sc reaction and ^{77}Rb was populated with an excitation energy of 71 MeV and $l_{\max} = 43\hbar$ through the ^{32}S + ^{45}Sc reaction. The typical flight time of ERs, formed in both the reactions, through HIRA was of the order of 0.86 μs.

A schematic layout of the experimental setup is shown in Fig. 1. For monitoring the elastically scattered beam two Si surface barrier detectors were kept inside the target chamber at $\pm 25^\circ$ with respect to the beam and at a distance of 10 cm from the target position. Charged particle spectra were obtained using a ΔE-E (25 μm-5 mm) Si surface barrier telescope detector setup kept at 40° with respect to the beam at a distance of 5.1 cm from the target position. The telescope detector was calibrated using ^{241}Am source. Neutron spectrum was recorded at 90° with respect to the beam using a NE213 liquid scintillator detector, having 3 in. diameter and 5 in. thickness, kept at a distance of 92 cm from the target position. The neutron detector is sensitive to both the neutrons and γ rays. Discrimination between neutrons and γ rays was achieved by the time of flight (TOF) technique and method of pulse shape discrimination (PSD) based on the zero crossover technique [23]. Figure 2 shows the separation between neutrons and γ rays obtained by using TOF and PSD spectra.

The energy threshold of the neutrons was kept at 0.5 MeV by calibrating the detector with standard γ-ray sources (^{137}Cs and ^{60}Co) [24]. The level of the background in the neutron spectra was estimated by taking a background run with a blank target. The observed background was negligible in the neutron spectra. In order to ascertain the statistical origin of the experimental data, the coincidence light particle spectra were obtained by gating with the ERs. For the detection of ERs, HIRA spectrometer was scanned for the charge states,

[1] $l_{\max}\hbar = \sqrt{2\mu(E_{\rm c.m.} - V_b)}(R + D_1)$, $V(b) = \frac{1.44 Z_P Z_T}{R + D_2}$, and $R = R_o((A_P)^{\frac{1}{3}} + (A_T)^{\frac{1}{3}})$ with $R_o = 1.18$, $D_1 = 0.8$, and $D_2 = 2.9 - 0.005(A_P + A_T)$.

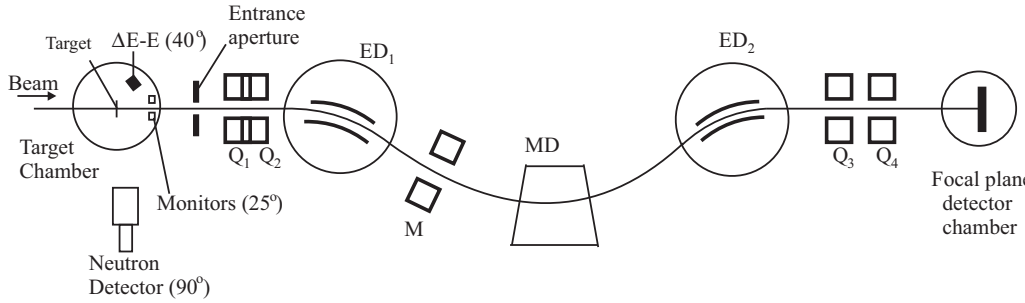

FIG. 1. The schematic layout of the experimental setup. Q, ED, M, and MD stand for magnetic quadrupole, electrostatic dipole, magnetic multipole, and magnetic dipole, respectively.

mass, and energy of ERs for both systems and set for the most dominant ER channel in each case. The ERs were separated from the intense beam-like particles by HIRA and were dispersed at the focal plane of HIRA according to their m/q values. The focal plane detector consisted of a multiwire proportional counter (MWPC) [25] having an active area of 6 in.$\times$2 in. The MWPC has a five electrode geometry namely two cathodes sandwiching two position electrodes and a central anode.

The TOF information of the ERs was obtained by setting a time-to-amplitude converter (TAC) using the anode signal of the MWPC as start and the delayed radio frequency (RF) signal as stop. A two-dimensional spectrum was generated using the TOF and energy loss of ERs (from the cathode of MWPC). The spectrum provides a clean separation of ERs from the beam-like particles as shown in Fig. 3. During the evaporation process, when there is an emission of a particle from CN the residue nucleus gets a recoil. This recoil will be negligible for the case of protons and neutrons. However, the recoil due to α-particle emission will be much larger and it may be possible that all the ERs may not be accepted by HIRA. So, for the exclusive measurement of light particle spectra, ERs were also measured at different angle settings of the HIRA from 0° to 12° with respect to the beam axis to take into account the recoil of ERs due to α-particle emission. The spectra recorded at each angle of HIRA were added to get the final spectra.

The data analysis has been performed using the CANDLE [26] software. Inclusive α-particle, proton, and neutron spectra are obtained from the respective detectors. The following subsections describe the procedure followed for the experimental data reduction.

A. Light particles evaporation spectra

The identification of α particles and protons has been carried out using the range-energy method. The data from the telescope is sorted to obtain separate lobes of different particles by plotting $(E + \Delta E)$ versus a characteristic particle identifier variable constructed as $[(E + \Delta E)^{1.58} - E^{1.58}]^{0.58}$. A suitable gate is applied to get the α-particle and proton spectra. The spectra thus obtained are the inclusive α-particle and proton spectra. The inclusive neutron TOF spectrum has been calibrated considering the prompt γ-ray peak as a reference. The calibrated neutron TOF spectrum was converted to neutron energy using the following relation:

$$E_n = \frac{1}{2} m \frac{d^2}{t^2}, \tag{1}$$

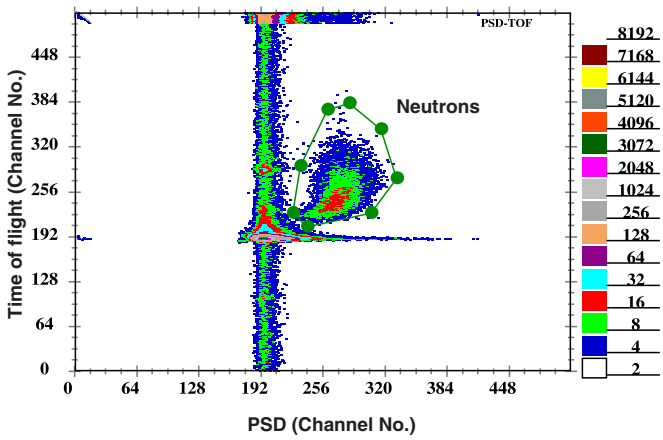

FIG. 2. (Color online) Two-dimensional plot of TOF vs PSD used to distinguish the neutrons from γ rays. The neutron lobe is marked with green dot-line markers.

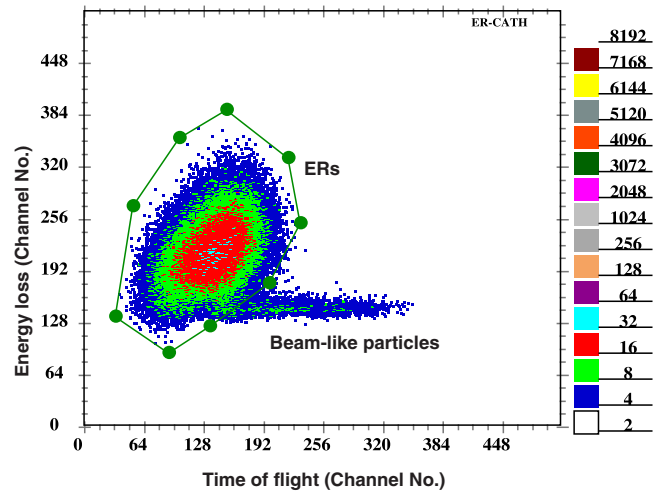

FIG. 3. (Color online) Two-dimensional spectrum showing the energy loss vs time of flight of ERs. The ER lobe is marked with green dot-line markers.

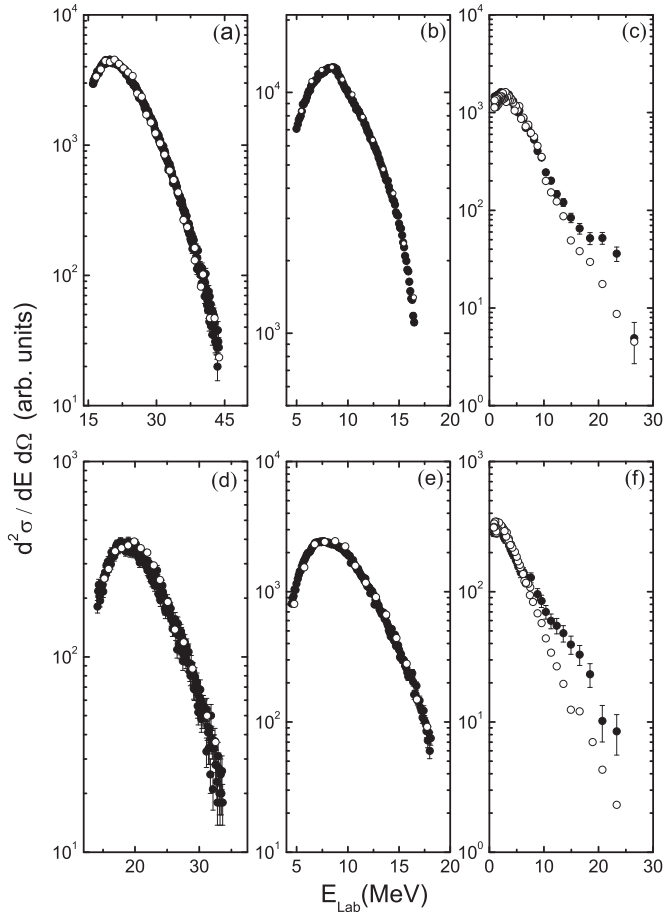

FIG. 4. (a)–(c) Upper panel shows the comparison of the inclusive and exclusive experimental spectra of (a) α particles and (b) protons at $\theta_{\rm lab} = 40^\circ$, (c) neutrons at $\theta_{\rm lab} = 90^\circ$ for the symmetric reaction ^{28}Si + ^{45}Sc at $E^* = 78$ MeV. The solid circles represent the inclusive data, and open circles represent the exclusive spectra. (d)–(f) The same as the upper panels but for the symmetric reaction ^{32}S + ^{45}Sc at $E^* = 71$ MeV.

where m is the mass of neutron, d is the flight path, and t is the time of flight. The efficiency of the neutron detector has been obtained using the Monte Carlo simulation based code MODEFF [27]. The efficiency values of the neutron detector depend on the neutron energy, scintillator geometry, and the neutron threshold. The simulated efficiencies are found to be in excellent agreement with the experimentally obtained efficiencies [28]. Separate exclusive spectra are also obtained by gating the particle spectra with the ERs detected at the focal plane of HIRA. Figure 4 shows the comparison of exclusive and inclusive spectra for the α particle, proton, and neutron for both the CN ^{73}Br and ^{77}Rb. As evident from the figure, the shapes are same for both the inclusive and exclusive spectra. Moreover for the neutron spectra a bump-like structure is seen in inclusive as well as exclusive spectra. The appearance of the bump gives a signature about the presence of the pre-equilibrium process [13]. For the theoretical analysis purpose, we have used the exclusive spectra.

B. Evaporation residue cross section

An attempt has also been made to obtain the fusion (= ER) cross sections from the present experimental measurement. The total ER cross sections can be calculated by the relation

$$\sigma_{\rm ER} = \frac{Y_{\rm ER}}{Y_{\rm Mon}} \frac{\Omega_{\rm Mon}}{\bar{\eta}_{\rm HIRA}} \left(\frac{d\sigma}{d\Omega_{\rm Mon}} \right)_{\rm Ruth}, \qquad (2)$$

where $Y_{\rm ER}$ is the ER yield at the focal plane of HIRA, $Y_{\rm Mon}$ is the elastically scattered events detected by the monitor detector, $(d\sigma/d\Omega_{\rm Mon})_{\rm Ruth}$ is the Rutherford scattering differential cross section, $\Omega_{\rm Mon}$ is the solid angle subtended by the monitor detector, and $\bar{\eta}_{\rm HIRA}$ is the average value of transmission efficiency of the ERs through HIRA. The transmission efficiency of each ER is given by the ratio of number of that particular ER reaching the focal plane to the total number of ERs emerging from the target. For the present work, we have calculated the value of the transmission efficiency of each ER using the semimicroscopic Monte Carlo code, TERS [29,30]. TERS generates the displacement, divergence, energy, and charge states of different ERs. Finally it calculates the ER trajectories through HIRA by first-order ion optical transfer matrices. The code has given good agreement with the measured efficiency values for different systems [31]. The average ER transmission efficiency through HIRA, $\bar{\eta}_{\rm HIRA}$, has been evaluated by taking the weighted average of $\eta_{\rm HIRA}$ for different ER channels. The relative population of individual ER channels has been taken from PACE3 [32]. The cross sections measured by the above procedure for the systems ^{32}S + ^{45}Sc and ^{28}Si + ^{45}Sc at 125 MeV have been found to be 600 ± 72 mb and 690 ± 83 mb, respectively. The observed values of the cross sections are found to be reduced in comparison to the those predicted by the Bass model [33]. This reduction in the cross section values hints at the possible reduction of the l values contributing to the fusion process.

III. THEORETICAL ANALYSIS AND RESULTS

The compound nucleus formation process and its decay is generally described by various approaches such as macroscopic theory [34], the statistical model [35], and full microscopic theory such as time-dependent Hartree-Fock (TDHF) [36]. In a macroscopic approach no dynamics of the reaction process is given but the choice of the co-ordinates that govern the evolution of the reaction is generally given as the input [37,38]. The use of the statistical model in describing the decay of the CN is quite successful even today [35]. Various statistical model based codes such as CASCADE [39], PACE [32], GEMINI++ [16], etc., are used extensively for the interpretation of the experimental data. However, it should be noted here that the history of the nucleus-nucleus collision, leading to a particular nuclear process can be best known by solving the TDHF equation. This method serves as an important platform for the fully microscopic many-body theory for heavy ion reactions at low energies. These calculations can be performed by using different parametrizations of the Skyrme interaction between the nucleons. The density distribution are obtained by squaring the time dependent wave functions. Different reaction channels, such as fusion, fission, and deep-inelastic

process, can be distinguished through these calculations. In recent years such calculations have evolved and been highly successful [37,40–44]. The predictions regarding the evolution and decay of the CN, including the full dynamics of the reaction process, from the fundamental theories like TDHF, are certainly desirable, but for the sake of simplicity we have used the statistical model based code CASCADE and the dynamical model code HICOL.

The important ingredients of the statistical model calculations are level density, deformation parameters, transmission coefficients, fission barrier height, inverse reaction cross sections, and spin distribution. In the next subsection we shall now describe the statistical model calculations based on the CASCADE code.

A. CASCADE statistical model calculations

The measured light particle evaporation spectra for both the systems are compared with the statistical model calculations using the transmission coefficients from the optical model for the spherical nuclei and the RLDM moment of inertia using default values of deformation parameters (δ_1 and δ_2), $l = l_{\max}$, and level density parameter 'a' $= A/8$ MeV^{-1}, see (Fig. 5).

It is observed that the experimental spectra are strongly deviating from the statistical model CASCADE calculations, especially, at higher energy sides of the spectra. These calculations overpredict the α-particle and proton spectra and underpredict the neutron spectra. To account for these deviations of the experimental spectra from the predictions of the CASCADE statistical model, we have carried out further analysis as described in the following subsections.

B. Statistical model calculations by rescaling the yrast line

In the CASCADE code, the effective rotational energy is parametrized as

$$E_I = \frac{\hbar^2 I(I+1)}{2\Im} = \frac{\hbar^2 I(I+1)}{2\Im_0(1+\delta_1 I^2+\delta_2 I^4)}, \qquad (3)$$

where δ_1 and δ_2 are the deformation parameters, $\Im_o$ is the rigid body moment of inertia, M is the mass of the nucleus, and R is the radius with $R_o = 1.25$ fm. For fitting the spectra, the spin dependent level density with E_I values generated with the increased values of δ_1 and δ_2 are introduced. It is observed that the statistical model calculations performed using $\delta_1 = 0.62\times10^{-04}$ and $\delta_2 = 0.70\times10^{-07}$ for the CN ^{73}Br and $\delta_1 = 1.5\times10^{-04}$ and $\delta_2 = 1.5\times10^{-07}$ for ^{77}Rb, with the optical model transmission coefficients for the spherical nuclei, $l = l_{\max}$ and 'a' $= A/8$ MeV^{-1}, produce a noticeable change in the slope of the high energy tail of the α-particle spectra without affecting the peak and the low energy part of the spectra for both systems as shown in Fig. 6. However, it does not explain the proton and neutron spectra. This increase in the values of δ_1 and δ_2 reduces the values of E_I for the higher spin states relative to those for the lower spin states. It raises the level density of high spin states relative to that of lower spin states in the residue nuclei and suppresses the available phase space for α-particle emission from high spin compound nuclear states. The suppression of first chance α-particle emission leads to the softening of the slope of the high energy part of the α-particle spectra and the low partial wave emission of neutrons and protons from the CN is enhanced. Table I lists the increased values of the deformation parameters required to fit the light particle evaporation spectra for the present systems and different systems existing in literature.

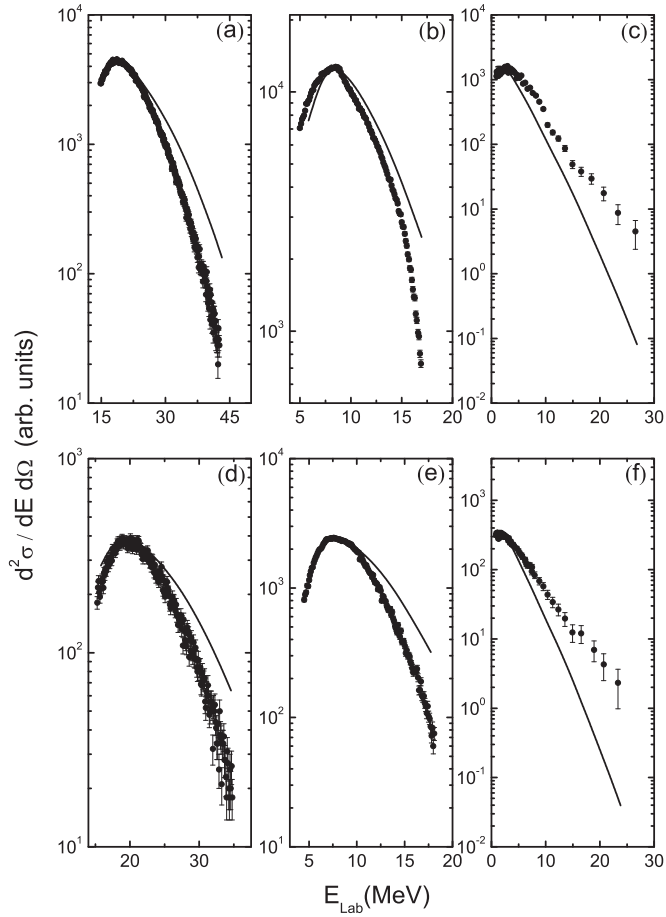

FIG. 5. (a)–(c) Upper panel shows the comparison of the experimental data (solid circles) with the conventional statistical model calculations (solid lines), as described in the text, for the symmetric reaction ^{28}Si + ^{45}Sc at $E^* = 78$ MeV (a) the α-particle spectrum and (b) the proton spectrum at $\theta_{\text{lab}} = 40^\circ$, (c) the neutron spectrum at $\theta_{\text{lab}} = 90^\circ$. (d)–(f) The same as for the upper panels but for the symmetric reaction ^{32}S + ^{45}Sc at $E^* = 71$ MeV.

The conventional statistical model cannot be applied to explain the evolution of a complex nuclear system formed in a heavy ion induced reaction. During the interaction process the energy of the projectile couples with the intrinsic degrees of freedom which leads to a dissipative behavior. As a result of dissipation, the thermal energy contained in the intrinsic degrees may change rapidly up to a substantial fraction of the coherent kinetic energy obtained in the macroscopic variables. Different dynamical models have been framed to account for the dissipative dynamics involved in the fusion process. We have tried to understand the observed deviations of the spectra by the Feldmeier one-body dissipation model calculations using the HICOL code based on the long mean free path of

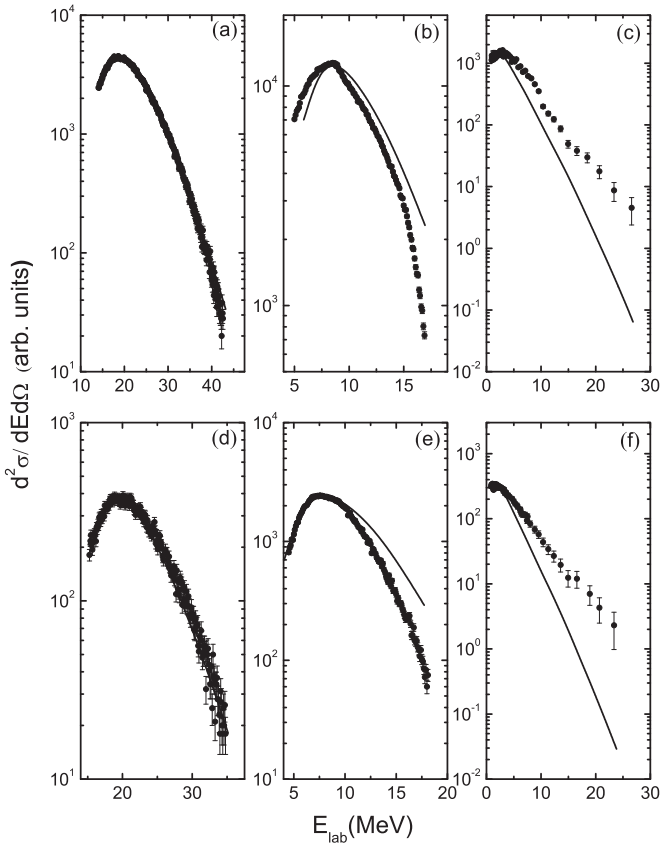

FIG. 6. (a)–(c) Upper panel shows the comparison of the experimental data (solid circles) with the statistical model calculations (solid lines) as described in the text, for the symmetric reaction $^{28}\mathrm{Si} + ^{45}\mathrm{Sc}$ at $E^* = 78$ MeV; (a) the α spectrum and (b) the proton spectrum at $\theta_{\mathrm{lab}} = 40^\circ$, (c) the neutron spectrum at $\theta_{\mathrm{lab}} = 90^\circ$.(d)–(f) The same as for the upper panels but for the symmetric reaction $^{32}\mathrm{S} + ^{45}\mathrm{Sc}$ at $E^* = 71$ MeV.

nucleons in their self-consistent one-body potential and the classical Swiatecki dynamical model calculations [20,21].

The results of HICOL calculations for both systems are shown in Figs. 7 and 8. In Figs. 7(a) and 8(a) the distance between the fusing nuclei 's' is plotted as a function of time for various values of l. The dashed line corresponds to closest distance of approach, $s = s_{\mathrm{crit}}$, which is taken as equal to the radius of the CN, $R = R_o A^{\frac{1}{3}}$. These plots reveal that for both systems the trajectories up to $l > 30\hbar$ do not approach $s = s_{\mathrm{crit}}$ and hence only the partial waves up to $l = 30\hbar$ fuse into the CN. This value of l is less than the $l = l_{\mathrm{max}}$ for both systems. The compound nucleus shape equilibration time for the fusing trajectories is about 40.6×10^{-22} s and 37.1×10^{-22} s for ^{73}Br and ^{77}Rb, respectively. The thermal excitation energy as a function of time is plotted in Figs. 7(b) and 8(b). The thermal equilibrium (90% of the final excitation energy) for various partial waves is approached within about 10×10^{-22} s. So these calculations indicate that the shape equilibration time is more than the thermal equilibrium process thereby suggesting that the dissipation hinders the shape equilibration more strongly than the thermal equilibration.

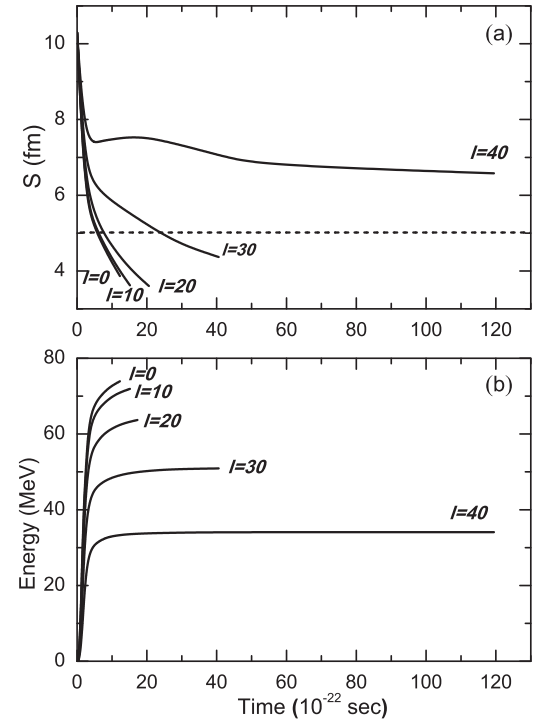

FIG. 7. (a) Calculated evolution of the separation 's' of colliding nuclei as a function of time and (b) calculated evolution of the excitation energy of colliding nuclei as a function of time for the symmetric reaction $^{28}\mathrm{Si} + ^{45}\mathrm{Sc}$. The dashed line corresponds to $s = s_{\mathrm{crit}}$.

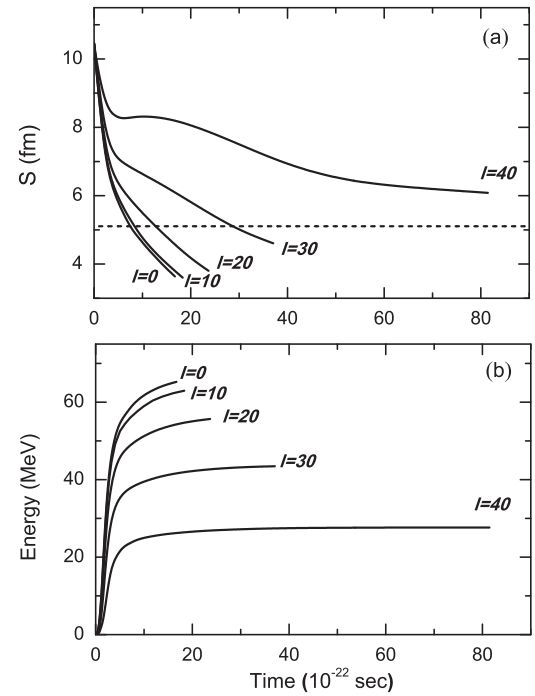

FIG. 8. Same as for Fig. 7 but for the system $^{32}\mathrm{S} + ^{45}\mathrm{Sc}$.

TABLE I. List of different systems along with the corresponding fitting parameters used to explain the experimental light particle spectra.

S.No.	System	Asymmetry parameter, α_{asym}	E^* (MeV)	Classical l_{max} ($\hbar$)	Spectra	δ_1	δ_2	HICOL l ($\hbar$)	'a' (MeV^{-1})	Reference
1	^{28}Si + ^{45}Sc	0.233	78	47	α	0.62×10^{-04}	0.70×10^{-07}			present work
					α			30		present work
					p				12.31	present work
					n				6.3	present work
2	^{32}S + ^{45}Sc	0.169	71	43	α	1.5×10^{-04}	1.5×10^{-07}			present work
					α			30		present work
					p				13.75	present work
					n				6.4	present work
3	^{32}S + ^{48}Ti	0.200	70	43	α	4.45×10^{-05}	5.0×10^{-08}			[6]
		0.200			α			30		[6]
					n				8	[8]
4	^{16}O + ^{64}Zn	0.600	75	43	α, p, n	1.45×10^{-05}	2.0×10^{-08}		10	[6,8]
5	^{34}S + ^{45}Sc	0.139	80	50	α	4.6×10^{-05}	4.9×10^{-08}			[5]
					α			35		[5]
					p			35		[5]
6	^{16}O + ^{63}Cu	0.594	85	50	α, p	1.66×10^{-05}	1.95×10^{-08}		9.87	[5]
7	^{28}Si + ^{27}Al	0.0182	84	42	α	1.78×10^{-04}	1.81×10^{-07}			[14]
					α			30		[3]
8	^{28}Si + ^{51}V	0.291	85	56	α			23		[3]
9	^{16}O + ^{54}Fe	0.543	85	34	α	2.45×10^{-05}	3.01×10^{-08}		8.75	[4]
10	^{31}P + ^{45}Sc	0.184	75	43	n				7.6	[9]
11	^{31}P + ^{27}Al	0.059	79.5	56	n				5.8	[10]

A comparison of the thermal and shape equilibration times for the present systems with asymmetric systems ^{16}O + ^{54}Fe [4] and ^{16}O + ^{63}Cu [5] populating CN with similar masses is shown in Table II. It can be seen that thermal equilibration for all the systems is achieved within 10×10^{-22} s but the shape equilibration time of the CN increases rapidly as we move from the asymmetric to the symmetric system. This delay in the evolution or equilibration process may result into some other reaction channels which the dynamical model does not take into account.

Another approach by Swiatecki [20,21], considers three milestone configurations in the potential energy surfaces of the colliding nuclei, namely the contact configuration for touching spheres, the conditional saddle point of fixed mass asymmetry, and unconditional saddle point for the symmetric mass split. The necessary condition for fusion is that the system passes over the conditional saddle point whereas the system must pass over the unconditional saddle point in order to form the CN. The unconditional saddle point potential energy curve versus mass asymmetry 'α_{asym}' shows a distinct peak in the potential energy curve at $\alpha_{asym} = \alpha_{BG}$, the Businaro-Gallone critical mass asymmetry [45]. For $\alpha_{asym} > \alpha_{BG}$, the interacting nuclei get captured immediately forming a mononucleus and then undergo equilibration. On the other hand for $\alpha_{asym} < \alpha_{BG}$, after the capture a dinuclear system is formed and the mass transfer takes place from the heavier to the lighter nuclei. Thus the equilibration process is slowed down and some other reaction processes (like pre-equilibrium processes) may open up. The angular momentum dependent α_{BG} calculations [46] have been performed for present compound systems for different values of l. For higher partial waves the value of α_{BG} starts approaching the value of α_{asym}, indicating that the fusion process follows a dynamically hindered path and their fusion is inhibited, thereby supporting the results from the HICOL code predictions. So, we have performed the statistical model calculations taking into account the nonfusion of the higher partial waves. These calculations are described in the next subsection.

TABLE II. Comparison of various parameters for the present systems and asymmetric systems of similar masses.

S.No.	System	E_{lab} (MeV)	E^* (MeV)	l_{max} ($\hbar$)	Thermal equilibration time ($\times10^{-22}$ s)	Shape equilibration time ($\times10^{-22}$ s)	HICOL predicted l value ($\hbar$)
1	^{28}Si + ^{45}Sc	125	78	47	6.0	40.6	30
2	^{32}S + ^{45}Sc	125	71	43	9.0	37.1	30
3	^{16}O + ^{54}Fe	110	85	48	5.0	26.0	48
4	^{16}O + ^{63}Cu	140	85	50	5.0	24.9	50

C. Statistical model calculations using HICOL predicted *l* value

The experimental α-particle, proton, and neutron spectra from both the reactions are compared with the statistical model predictions, carried out using the HICOL predicted $l = 30\hbar$ (as suggested by other dynamical model also), transmission coefficients from the optical model for the spherical nuclei, and the RLDM moment of inertia using default values of δ_1 and δ_2 and 'a' $= A/8$ MeV^{-1} as shown in Fig. 9. It is evident that the model predicted α-particle spectra are in good agreement with the experimental spectra. This approach can be taken as an alternative of rescaling the yrast line, such that E_I for higher spin states is diminished in comparison to E_I for lower spin states. The reduction in the l values, as predicted by HICOL, is consistence with the observed reduction in the cross sections as compared to the Bass model predictions [33], for both the systems as described in Sec. II B. However, this approach is still unable to explain the anomalous deviation of the experimental proton and neutron spectra. The HICOL predicted l values for different systems existing in literature are listed in Table I.

D. Statistical model calculations using Gilbert and Cameron '*a*'

As an alternate approach to explain the experimental light particle spectra, statistical model calculations are performed using Gilbert and Cameron (GC) [47] level density parameter. The GC prescriptions defines the level density parameter as

$$\frac{a}{A} = 0.00917S + 0.142, \tag{4}$$

where $S = S(N) + S(Z)$ is the total shell correction, and $S(N)$ and $S(Z)$ are the shell corrections for neutrons and protons, respectively. The calculated GC values in the mass region of 70–80 fall around 12 MeV^{-1}. The statistical model calculations are performed with 'a' as a free parameter and using the transmission coefficients from the optical model for the spherical nuclei, the RLDM moment of inertia using default values of δ_1 and δ_2 and $l = l_{\max}$. It is observed that this approach explains the experimental proton spectra (for 'a' $=$ 12.31 MeV^{-1} and 13.75 MeV^{-1} for the systems ^{28}Si $+$ ^{45}Sc and ^{32}S $+$ ^{45}Sc, respectively) but is unable to explain the α-particle and neutron spectra as shown in Fig. 10. The values of 'a' required to explain the proton spectra for both the systems are in good agreement with the Gilbert and Cameron values. These

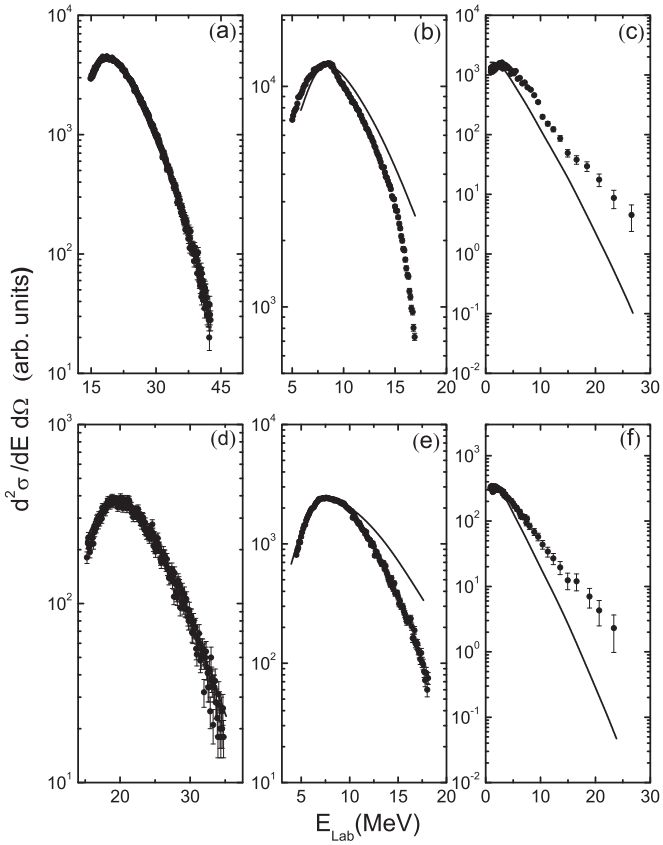

FIG. 9. (a)–(c) Upper panel shows the comparison of the experimental data (solid circles) with the statistical model calculations (solid lines) as described in the text, for the symmetric system ^{28}Si $+$ ^{45}Sc at $E^* = 78$ MeV; (a) the α-particle spectrum and (b) the proton spectrum at $\theta_{\text{lab}} = 40^\circ$, (c) the neutron spectrum at $\theta_{\text{lab}} = 90^\circ$. (d)–(f) The same as for the upper panels but for the symmetric system ^{32}S $+$ ^{45}Sc at $E^* = 71$ MeV.

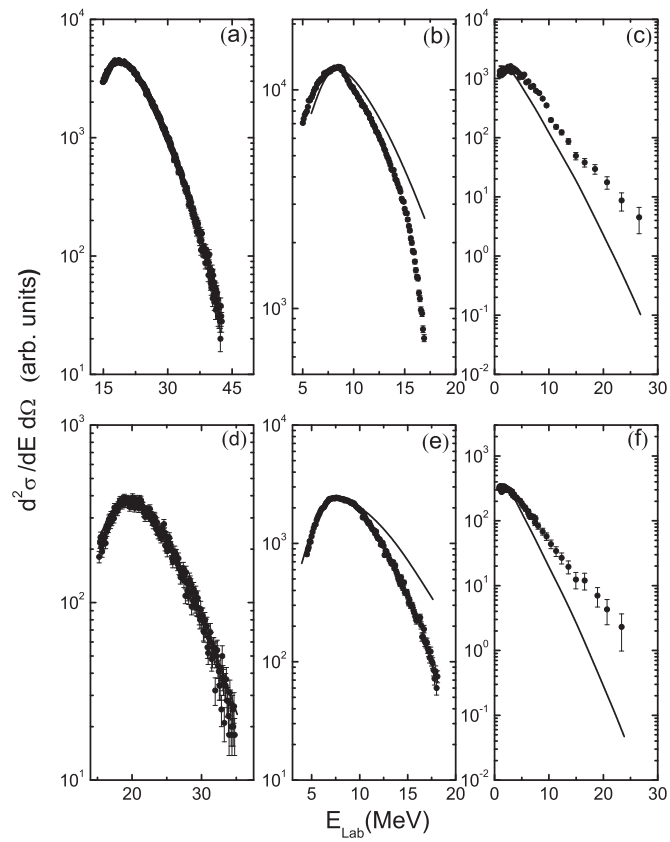

FIG. 10. (a)–(c) Upper panel shows the comparison of the experimental data (solid circles) with the statistical model calculations (solid line) as described in the text, for symmetric reaction ^{28}Si $+$ ^{45}Sc at $E^* = 78$ MeV; (a) the α-particle spectrum and (b) the proton spectrum at $\theta_{\text{lab}} = 40^\circ$, (c) the neutron spectrum at $\theta_{\text{lab}} = 90^\circ$. (d)–(f) The same as for the upper panels but for the symmetric reaction ^{32}S $+$ ^{45}Sc at $E^* = 71$ MeV.

calculations result in the softening of the higher energy side of the proton spectra and the theoretical spectra come closer to the experimental spectra, except over a very small energy range closer to higher end point energy.

E. Statistical model calculations using lowered value of '*a*'

While attempting to fit the experimental spectra using '*a*' as free parameter and transmission coefficients from the optical model for the spherical nuclei, the RLDM moment of inertia using default values of δ_1 and δ_2 and $l = l_{max}$, it is observed that the reasonable fit to neutron spectra can be obtained using a lower value of level density parameter ('*a*' = 6.3 MeV^{-1} and '*a*' = 6.4 MeV^{-1} for ^{73}Br and ^{77}Rb, respectively). Figure 11 shows the comparison of the experimental results with the theoretical calculations. Here it must be added that a considerable deviation from model predictions has been observed at the higher energy tail of the spectra. The observed deviation cannot be explained even by lowering the value of '*a*' which clearly indicates the significant contribution of nonstatistical neutrons at the high energy tail of spectra. However these values of '*a*' are not able to fit the

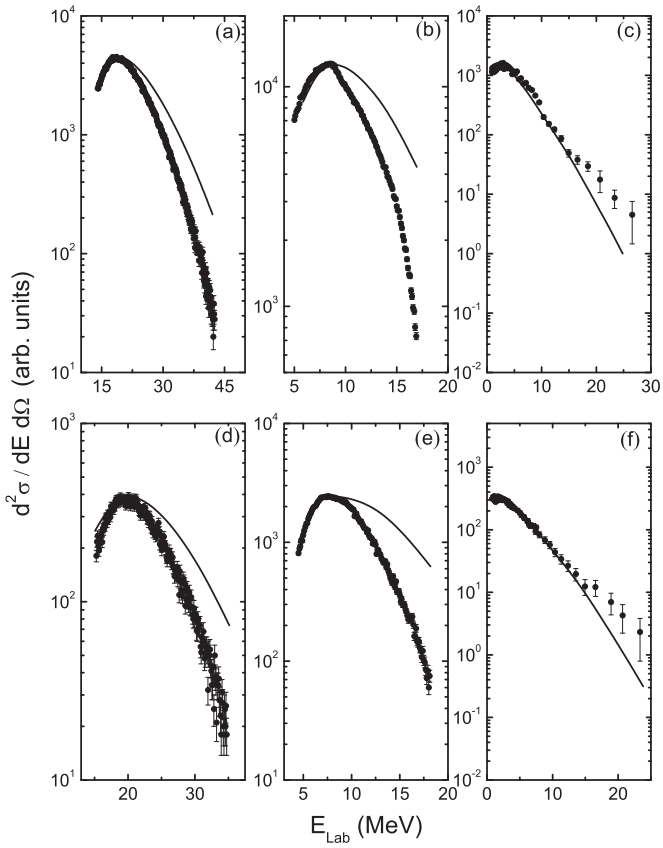

FIG. 11. (a)–(c) Upper panel shows the comparison of the experimental data (solid circles) with the statistical model calculations (solid lines) as described in the text, for symmetric reaction ^{28}Si + ^{45}Sc at $E^* = 78$ MeV; (a) the α-particle spectrum and (b) the proton spectrum at $\theta_{lab} = 40^\circ$, (c) the neutron spectrum $\theta_{lab} = 90^\circ$. (d)–(f) The same as for the upper panels but for the symmetric reaction ^{32}S + ^{45}Sc at $E^* = 71$ MeV.

α-particle and proton spectra. A summary of the values of '*a*' used for explaining the observed deviations in neutron spectra for different symmetric systems is given in Table I.

IV. DISCUSSION

The inclusive as well as exclusive (ER gated) α-particle, proton, and neutron spectra from the CN ^{73}Br and ^{77}Rb have been measured. The experimental light particle evaporation spectra have been compared with the statistical model predictions using RLDM values of moment of inertia, optical model transmission coefficients for spherical nuclei, '*a*' = $A/8$, and $l = l_{max}$. It is observed that the statistical model could not explain the observed experimental spectra.

Similar observations have been reported for different symmetric systems [1–10]. Unlike most of the earlier measurements, the present work deals with the exclusive measurement for all the decay channels. Similar deviations from the statistical model predictions are observed both in inclusive and exclusive measurements, which suggest that there is no interference from other reaction channels. To explain these deviations different techniques have been used. The use of the increased value of deformation parameters explains the α-particle spectra. Application of dynamical theories [18,20,21] to the reactions under study suggests that the fusion of higher partial waves ($l \backsimeq 30\hbar$–$40\hbar$) is strongly inhibited due to delayed shape equilibrium and results in the formation of deformed intermediate dinuclear system. The dynamical deformation modifies the yrast line and enhances the level density of high spin states compared to the low spin states over the expected values in the spherical or equilibrated CN. Besides this, the dynamical deformation increases the binding energy for α particles and protons significantly while for neutrons the binding energy decreases with an increase in deformation [48] in comparison to the spherical or equilibrated shape. Both of these factors inhibit the participation of α-particle emission through the dinuclear system formed by higher partial waves. So, we conclude that as far as the deviations of α-particle spectra from the statistical model predictions are concerned, these arise from the fusion of lower partial waves and there is no contribution from higher partial waves. The α-particle spectra are fitted by using the lower value of l ($30\hbar$) as suggested by the dynamical model. However, both these approaches could not explain the proton and neutron spectra.

Different values of '*a*' were used to explain the proton and neutron spectra. A comparison between the neutron and proton spectra reveals that for neutrons the effective '*a*' is lower while for protons it is higher than conventional value '*a*' = $A/8$ MeV^{-1}. It indicates that the neutron and proton spectra have the contribution from higher partial waves. This results in the modification of level density of the CN which indicates there is pre-equilibrium contributions from the higher partial waves over the different energy ranges of the tail portion of the spectra. We observe that the thermal equilibrium is quite fast and is completed to about 90% level within 10^{-22} s, however the shape equilibrium is delayed significantly by about 10^{-21} s as shown in Figs. 7 and 8. Therefore we conclude that the delayed shape equilibrium process of the remaining 10% of the excitation energy may facilitate the occurrence

of multistep compound (MSC) process [49,50] resulting in pre-equilibrium. However, due to the difference in binding energy in the deformed system the effective contribution from neutrons and protons will be different [48]. The contribution of neutrons will be dominant at the higher side of the tail of the spectra while for protons the contribution towards the pre-equilibrium is from the lower energy side of the tail of the spectra. So, the pre-equilibrium type of enhanced contribution of the neutron spectra at the high energy tail arises from the MSC process. The possibility of the existence of deep inelastic reactions is ignored as there is no effective decrease in the thermal excitation energy with the evolution time.

So, the consistent picture for explaining the deviations of the experimental spectra can be explained in terms of the dynamical evolution of the fusion process. The dynamical hindrance of the fusion of higher partial waves inhibits their contribution to the α-particle spectra. This approach is similar to the use of modified spin dependent level density which results in the enhancement of level density of higher spin states in the residual nucleus. The higher partial waves lead to MSC process [49,50] resulting in the pre-equilibrium contribution to neutron and proton spectra thereby modifying the effective level density of the residual nuclei.

V. SUMMARY AND CONCLUSIONS

Inclusive and exclusive light particle evaporation spectra are analyzed for the symmetric systems $^{28}\mathrm{Si} + ^{45}\mathrm{Sc}$ and $^{32}\mathrm{S} + ^{45}\mathrm{Sc}$. For both the systems, anomalous deviations are seen at the higher energy side of the experimental evaporation spectra as compared to the statistical model predictions. Different calculations are performed as an effort to explain the observed experimental spectra. These calculations suggest that the higher partial waves are not contributing to the fusion due to dynamical hindrance and the shape equilibration is delayed resulting in the formation of a dinuclear system having enhanced level density of higher spin states as compared to the lower spin states. The binding energy for charged particles increases and for neutrons the binding energy decreases. So the α-particle spectra are explained by considering the delayed fusion. The deviation of the protons and neutrons results from the MSC process resulting in pre-equilibrium. However, due to lower binding energy, neutron emission dominates over the protons emission resulting in the enhanced 'a' value for the protons and lowered value of 'a' for the neutrons. However to establish the presence of the MSC process resulting in pre-equilibrium to neutron and proton spectra, detailed refined angular distribution, multiplicity, spin distribution, and cross section measurements and their variations with energy, angular momentum, and asymmetry of the entrance channel and their comparison with the MSC process based calculations are required. In addition to this, the interpretation of fusion of different relatively symmetric systems should be made in terms of TDHF theory. Different improved versions of this theory are available now and it seems that these calculations may provide a more realistic outlook for the reaction mechanism of heavy ion induced reactions.

ACKNOWLEDGMENTS

The authors thank the accelerator crew of IUAC, New Delhi for providing beams of excellent quality throughout the experiment. Help received from T. Varughese in setting up the experiment is acknowledged. The authors are grateful to Dr. Santanu Pal and Dr. M. B. Chatterjee for stimulating discussions. One of the authors (M.K.) would like to thank University Grants Commission (UGC) for the financial assistance. This work is supported by the IUAC, New Delhi UFR grant no. UFR-44311.

[1] J. R. Huizenga, A. N. Behkami, I. M. Govil, W. U. Schroder, and J. Toke, Phys. Rev. C **40**, 668 (1989).
[2] I. M. Govil, Pramana **53**, 381 (1999).
[3] I. M. Govil, R. Singh, A. Kumar, J. Kaur, A. K. Sinha, N. Madhavan, D. O. Kataria, P. Sugathan, S. K. Kataria, K. Kumar, Bency John, and G. V. Ravi Prasad, Phys. Rev. C **57**, 1269 (1998).
[4] I. M. Govil, R. Singh, A. Kumar, Ajay Kumar, G. Singh, S. K. Kataria, and S. K. Datta, Phys. Rev. C **62**, 064606 (2000).
[5] J. Kaur, I. M. Govil, G. Singh, Ajay Kumar, A. Kumar, B. R. Behera, and S. K. Datta, Phys. Rev. C **66**, 034601 (2002).
[6] J. Kaur, A. Kumar, Ajay Kumar, G. Singh, S. K. Datta, and I. M. Govil, Phys. Rev. C **70**, 017601 (2004).
[7] R. K. Choudhury, P. L. Gonthier, K. Hagel, M. N. Namboodiri, J. B. Natowitz, L. Adler, S. Simon, S. Kniffen, and G. Berkowitz, Phys. Lett. B **143**, 74 (1984).
[8] Ajay Kumar, A. Kumar, G. Singh, B. K. Yogi, Rakesh Kumar, S. K. Datta, M. B. Chatterjee, and I. M. Govil, Phys. Rev. C **68**, 034603 (2003).
[9] Ajay Kumar, A. Kumar, G. Singh, Hardev Singh, R. P. Singh, Rakesh Kumar, K. S. Golda, S. K. Datta, and I. M. Govil, Phys. Rev. C **70**, 044607 (2004).
[10] Ajay Kumar, Hardev Singh, Rajesh Kumar, I. M. Govil, R. P. Singh, Rakesh Kumar, B. K. Yogi, K. S. Golda, S. K. Datta, and G. Viesti, Nucl. Phys. A **831**, 137 (2009).
[11] B. Fornal, G. Prete, G. Nebbia, F. Trotti, G. Viesti, D. Fabris, K. Hagel, and J. B. Natowitz, Phys. Rev. C **37**, 2624 (1988).
[12] B. Fornal, F. Gramegna, G. Prete, G. Nebbia, R. Smith, G. D'Erasmo, L. Fiore, A. Pantaleo, G. Viesti, P. Blasi, F. Lucarelli, I. Iori, and A. Moroni, Phys. Rev. C **41**, 127 (1990).
[13] A. Gavron, J. R. Beene, R. L. Ferguson, F. E. Obenshain, F. Plasil, G. R. Young, G. A. Petitt, K. G. Young, M. Jaaskelainen, D. G. Sarantites, and C. F. Maguire, Phys. Rev. C **24**, 2048 (1981).
[14] D. K. Agnihotri, A. Kumar, K. C. Jain, K. P. Singh, G. Singh, D. Kabiraj, D. K. Avasthi, and I. M. Govil, Phy. Lett. B **307**, 283 (1993).

[15] B. Fornal, G. Viesti, G. Nebbia, G. Prete, and J. B. Natowitz, Phys. Rev. C **40**, 664 (1989).
[16] R. J. Charity, Phys. Rev. C **82**, 014610 (2010).
[17] S. Kundu, C. Bhattacharya, S. Bhattacharya, T. K. Rana, K. Banerjee, S. Muhkopadhayay, D. Gupta, A. Dey, and R. Saha, Phys. Rev. C **87**, 024602 (2013).
[18] H. Feldmeier, Rep. Prog. Phys. **50**, 915 (1987).
[19] A. Saxena, A. Chatterjee, R. K. Choudhury, S. S. Kapoor, and D. M. Nadkarni, Phys. Rev. C **49**, 932 (1994).
[20] W. J. Swiatecki, Nucl. Phys. A **376**, 275 (1982).
[21] W. J. Swiatecki, Nucl. Phys. A **428**, 199 (1984).
[22] A. K. Sinha, N. Madhavan, J. J. Das, P. Sugathan, D. O. Kataria, A. P. Patro, and G. K. Mehta, Nucl. Instrum. Methods Phys. Res. A **339**, 543 (1994).
[23] S. Venkataramanan, Arti Gupta, K. S. Golda, Hardev Singh, Rakesh Kumar, R. P. Singh, and R. K. Bhowmik, Nucl. Instrum. Methods Phys. Res. A **596**, 248 (2008).
[24] T. G. Masterson, Nucl. Instrum. Methods **88**, 61 (1970).
[25] Akhil Jhingan, P. Sugathan, Ranjeet Dalal, T. Varughese, H. Singh, J. Gehlot, S. Nath, J. J. Das, N. Madhavan, R. P. Singh, P. Shidling, B. R. Behera, and S. K. Mandal, Proceedings of the DAE Symposium on Nuclear Physics **52**, 585 (2007).
[26] E. T. Subramaniam, B. P. A. Kumar, and R. K. Bhowmik (unpublished).
[27] R. A. Cecil, B. D. Anderson, and R. Madey, Nucl. Instrum. Methods **161**, 439 (1979).
[28] V. Singh, B. R. Behera, M. Kaur, A. Kumar, P. Sugathan, K. S. Golda, A. Jhingan, M. B. Chatterjee, R. K. Bhowmik, D. Siwal, S. Goyal, J. Sadhukhan, S. Pal, A. Saxena, S. Santra, and S. Kailas, Phys. Rev. C **87**, 064601 (2013).
[29] S. Nath, Comput. Phys. Commun. **180**, 2392 (2009).
[30] S. Nath, Comput. Phys. Commun. **179**, 492 (2008).
[31] S. Nath, Nucl. Instrum. Methods Phys. Res. A **576**, 403 (2007).
[32] A. Gavron, Phys. Rev. C **21**, 230 (1980).
[33] R. Bass, Nucl. Phys. A **231**, 45 (1974); Phys. Lett. B **47**, 139 (1973).
[34] J. R. Nix and A. J. Sierk, Phys. Rev. C **15**, 2072 (1977).
[35] R. G. Stokstad, in *Treatise in Heavy Ion Science*, edited by D. A. Bromley (Plenum, New York, 1985), Vol. 3, p. 83.
[36] K. T. R. Davies, K. R. S. Devi, S. E. Koonin, and M. R. Strayer, in [35], Vol. 3, p. 3.
[37] A. S. Umar and V. E. Oberacker, Phys. Rev. C **73**, 054607 (2006).
[38] J. Randrup, Nucl. Phys. A **307**, 319 (1978); **327**, 490 (1979).
[39] F. Pühlhofer, Nucl. Phys. A **280**, 267 (1977).
[40] A. S. Umar, M. R. Strayer, R. Y. Cusson, P.-G. Reinhard, and D. A. Bromley, Phys. Rev. C **32**, 172 (1985).
[41] R. T. deSouza, S. Hudan, V. E. Oberacker, and A. S. Umar, Phys. Rev. C **88**, 014602 (2013).
[42] V. E. Oberacker and A. S. Umar, Phys. Rev. C **87**, 034611 (2013).
[43] C. Simenel, R. Keser, A. S. Umar, and V. E. Oberacker, Phys. Rev. C **88**, 024617 (2013).
[44] R. Keser, A. S. Umar, and V. E. Oberacker, Phys. Rev. C **85**, 044606 (2012).
[45] U. L. Businaro and S. Gallone, Nuovo Cim. II **1**, 629 (1955); **1**, 1277 (1955); **5**, 315 (1957).
[46] M. Abe, KEK report 86-26, KEK TH-28 (1986).
[47] A. Gilbert and A. G. W. Cameron, Can. J. Phys. **43**, 1446 (1965).
[48] J. P. Lestone, Phys. Rev. Lett. **70**, 2245 (1993).
[49] M. Herman, R. Capote, B. V. Carlson, P. Oblozinsky, M. Sin, A. Trkov, H. Wienke, and V. Zerkin, Nucl. Data Sheets, **108**, 2655 (2007).
[50] H. S. Hans, Gulzar Singh, A. Kumar, K. P. Singh, B. R. Behera, and Sudip Ghosh, Phys. Rev. C **85**, 054614 (2012).